Petroleum Science 21 (2024) 1405–1414

Contents lists available at ScienceDirect

Petroleum Science

journal homepage: www.keaipublishing.com/en/journals/petroleum-science

Original Paper

Towards the insights into the deactivation behavior of acetylene hydrogenation catalyst

Hai-Xia Su [a, b], Yang Jiao [b], Jian-Gong Shi [b], Zhi-Wei Yuan [b], Di Zhang [a], Xu-Peng Wang [a], Jing Ren [b], Dan Liu [c], Jian-Zhou Gui [a, *], Hai-Yang Gao [a], Xiao-Li Xu [b]

[a] State Key Laboratory of Separation Membranes & Membrane Processes, Tianjin Key Laboratory of Green Chemical Technology and Process Engineering, School of Material Science and Engineering, Tiangong University, Tianjin, 300387, China
[b] Institute of Engineering Technology, Sinopec Catalyst Co., Ltd, Beijing, 101100, China
[c] State Key Laboratory of Separation Membranes and Membrane Processes, Tianjin Key Laboratory of Green Chemical Technology and Process Engineering, School of Chemistry, Tiangong University, Tianjin, 300387, China

ARTICLE INFO

Article history:
Received 16 March 2023
Received in revised form
25 June 2023
Accepted 16 October 2023
Available online 29 October 2023

Edited by Jia-Jia Fei and Min Li

Keywords:
Acetylene
Hydrogenation
Green oil
Carbon deposit
Sintering
Catalyst deactivation

ABSTRACT

A series of model catalysts were obtained by treating commercial fresh and spent catalysts unloaded from the factory with different methods, including green oil dipping, extraction and high-temperature regeneration; finally, the deactivation behavior of the commercial catalyst for acetylene hydrogenation were studied. The influence of various possible deactivation factors on the catalytic performance was elucidated via detailed structural characterization, surface composition analysis, and activity evaluation. The results showed that green oil, carbon deposit and sintering of active metal were the main reasons for deactivation, among which green oil and carbon deposit led to rapid deactivation, while the activity could be recovered after regeneration by high-temperature calcination. The sintering of active metal components was attributed to the high-temperature regeneration in hydrothermal conditions, which was slow but irreversible and accounted for permanent deactivation. Thus, optimizing the regeneration is expected to extend the service life of the commercial catalyst.

1. Introduction

As an important chemical raw material, ethylene is widely used in the production of a variety of high-value-added polyolefin products and is known as the cornerstone of the modern chemical industry. Generally, ethylene is produced by naphtha cracking in industry. However, the obtained ethylene inevitably contains some acetylene (about 0.3–3 *v*%) (Zhou et al., 2022); which can poison the Ziegler-Natta ethylene polymerization catalyst (Ru, 2021) and lead to a decrease in catalyst performance. To ensure the polymerization proceeds smoothly, the content of acetylene needs to be lower than 1 ppm (Wu et al., 2019), so it is necessary to take effective methods to eliminate the contaminating acetylene in ethylene (Hu et al., 2021; Huang et al., 2018; Li et al., 2019a; Wang et al., 2018; Chen et al., 2022a). Hence, it is necessary to take effective methods to eliminate acetylene. Selective hydrogenation of acetylene to ethylene is generally adopted in the industry. At present, commercial acetylene hydrogenation catalysts (also known as C2 selective hydrogenation catalysts) are alumina-supported Pd catalysts (Chen et al., 2022b; Hou et al., 2023; Liu et al., 2022; Ru, 2021; Tan et al., 2023; Yang et al., 2021; Zhang et al., 2022). Among them, Pd–Ag bimetallic catalyst is the most widely used (Zhang et al., 2018). Although the Pd–Ag catalyst exhibits good activity and selectivity, it is prone to inactivation (Guo et al., 2021; Huang and Chen, 2022; Li et al., 2019b; Melnikov et al., 2020; Méndez et al., 2021; Qi et al., 2021; Rassolov et al., 2020; Zhou et al., 2020). In order to obtain a long-lifetime catalyst, it is important to conduct a detailed study about the deactivation of the catalyst (Ren et al., 2021; Shi et al., 2022a, b, c, d, e).

Many researchers have devoted themselves to the deactivation of C2 catalysts (Hansen et al., 2013; Ma et al., 2020; Forzatti and Lietti, 1999; Kim et al., 2003). It reveals that acetylene tends to polymerize to form green oil (Zhou et al., 2022; Huang and Chen, 2022; Zhang et al., 2016). Green oil is a kind of liquid

* Corresponding author.
E-mail address: guijianzhou@tiangong.edu.cn (J.-Z. Gui).

https://doi.org/10.1016/j.petsci.2023.10.012

hydrocarbon with complicated compositions, which accumulates in the pore and on the surface of the catalyst, covering the active center and resulting in the deactivation of the catalyst (Borodziński and Bond, 2006; Huang and Chen, 2022; López and Vargas-Fuentes, 2012; Yang et al., 2013). Sarkany et al. (1984) stated that green oil covered the active sites of the catalyst and thereby decreased the activity. But it had little influence on product distribution. Wang (1995) concluded that the deposited green oil blocked the pore of the catalyst, which was an essential reason for the deactivation of the catalyst. Abdulrasheed et al. (2019) claimed that carbon deposit was an important factor in catalyst deactivation. Carbon deposits can not only cover the catalyst surface and the active metal sites but also form filamentous carbon species, which accumulate in catalyst pores, resulting in catalyst rupture and abrasion, reactor blockage, and activity decay. Tan et al. (2009) also stated that the formation of coke was the main cause of catalyst deactivation.

Sintering of active metal components is another important factor, leading to catalyst deactivation (Tan et al., 2009; Zhou et al., 2022). Forzatti and Lietti (1999) stated that sintering reduced the active metal-specific surface area and the number of active sites, leading to the deactivation of the catalyst. Zhang et al. (2017) investigated the relationship between green oil and catalyst activity using the spent catalysts at varying times on stream. They found that green oil only led to the temporary deactivation of the catalyst, while the sintering of Pd particles and loss of Ag were the main reasons for the permanent deactivation. Kim et al. (2003) pointed out that the sintering of Pd particles occurred during catalyst burning in the air during repeated cycles, which caused the deactivation of the catalyst. Hansen et al. (2013) divided the sintering process into three phases. Phase I involves a rapid loss in catalyst activity (or surface area), then sintering slows down in Phase II, and finally, the catalyst may reach a stable performance in Phase III.

Previous studies on the deactivation of Pd–Ag catalysts give many clues for the research and development of C2 catalysts. However, most of these studies were based on laboratory catalysts in micro-reactors (Che et al., 2020; Dehghani et al., 2019; Glyzdova et al., 2020a, b, 2021; Gonçalves et al., 2020; Ravindran et al., 2023; Wang et al., 2020). Due to the differences in operating conditions between the plant and the laboratory, this work is based on evaluating a commercial catalyst on an industrial scale, which holds the promise for understanding deactivation in large-scale operations. This will guide the development of new catalysts and the optimization of production processes. In this study, the deactivate behavior of the catalyst was studied in detail using the fresh commercial catalyst, the industrial spent catalyst, and a series of derived model catalysts, aiming to develop long-lifetime catalysts.

2. Experimental

2.1. Model catalysts

The used catalyst is commercially available. In this study, the fresh catalyst is denoted as Cat-1, and the spent catalyst is denoted as Cat-2. Cat-2, regenerated at high temperatures for many cycles, was permanently deactivated and unloaded from an industrial plant. Cat-3 was obtained by fully dipping the fresh catalyst Cat-1 in green oil from an industrial plant, which was only affected by green oil. Cat-4 was obtained by fully extracting green oil deposited in Cat-3 by a Soxhlet extractor with cyclohexane as solvent. The green oil accumulated in Cat-2 was fully extracted by Soxhlet extractor with toluene as solvent, and the obtained catalyst was denoted as Cat-5. Spent catalyst Cat-2 was calcined in the air at 500 °C for 4 h to remove green oil and carbon deposit completely, and the obtained catalyst was denoted as Cat-6. Catalyst Cat-7 was obtained by regenerating Cat-2 at industrial regeneration conditions (calcination at 500 °C in the air & steam) with a prolonged hydrothermal treating time of 48 h. The model catalysts, corresponding treatments, the main influencing factors and the relationships among them are shown in Fig. 1.

2.2. Catalytic performance

Catalytic evaluations were performed in a continuous flow fixed-bed microreactor. 0.75 g catalyst was loaded in the isothermal zone. Prior to the reaction, the catalyst was in-situ activated by 99.999% H_2 at 120 °C for 4 h at the gas hourly space velocity (GHSV) of 960 h^{-1}. After activation, the system was cooled down to 50 °C in the reducing gas flow, and then the inlet gas was switched to feed gas with the composition of 0.5 vol% acetylene, 0.7 vol% hydrogen, 6 vol% ethane, and 93.5 vol% ethylene. Usually, the catalytic reaction in the industrial scale is taken to ensure 100% of acetylene conversion, and the effect of the small amount of ethane produced by excess hydrogenation can be neglected. Therefore, under industrial working conditions, it is difficult to discriminate the catalytic

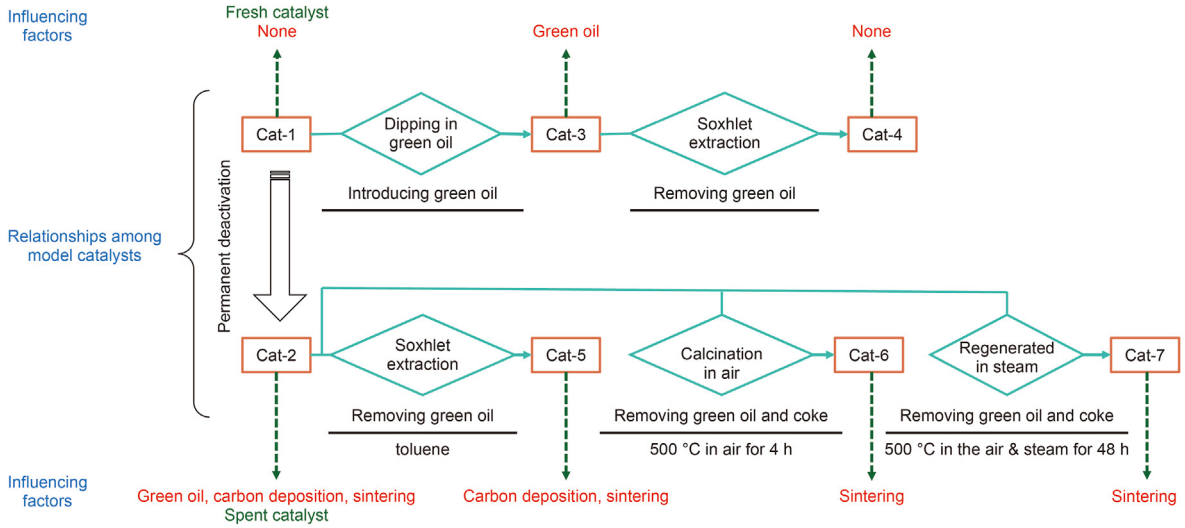

Fig. 1. The relationships among model catalysts with the corresponding treatments and the main influencing factors.

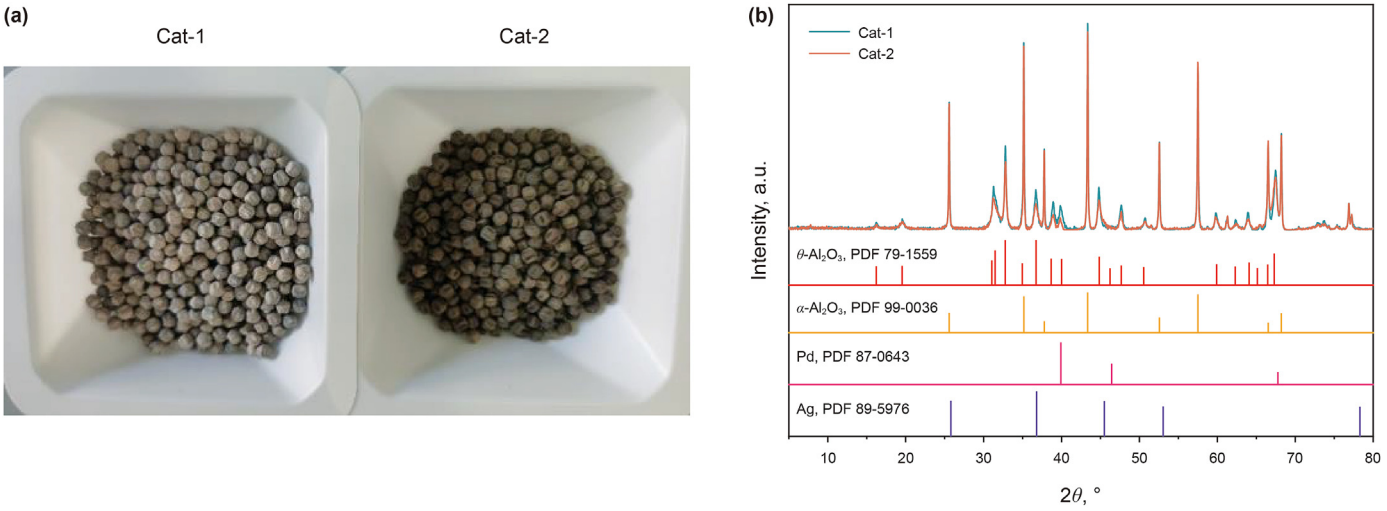

Fig. 2. (**a**) Photos of Cat-1 and Cat-2, (**b**) XRD patterns of Cat-1 and Cat-2.

activity change of the catalyst samples after different treatments. In order to enhance the performance difference between the series of catalyst samples, the evaluation was conducted at an enlarged GHSV, and the working condition is as follows: 1.5 MPa, GHSV 6000 h^{-1}, at a temperature of 50, 60, 70, 80, 90 °C. The tail gas was analyzed by online gas chromatography. Acetylene conversion and catalytic selectivity were calculated by Eqs. (1) and (2), as follows:

$$\text{Conversion} = \frac{C_{\text{Acetylene,feed gas}} - C_{\text{Acetylene,feed gas}}}{C_{\text{Acetylene,feed gas}}} \times 100\% \quad (1)$$

$$\text{Selectivity} = \frac{C_{\text{Ethylene,product}} - C_{\text{Ethylene,feed gas}}}{C_{\text{Acetylene,feed gas}} - C_{\text{Acetylene,feed gas}}} \times 100\% \quad (2)$$

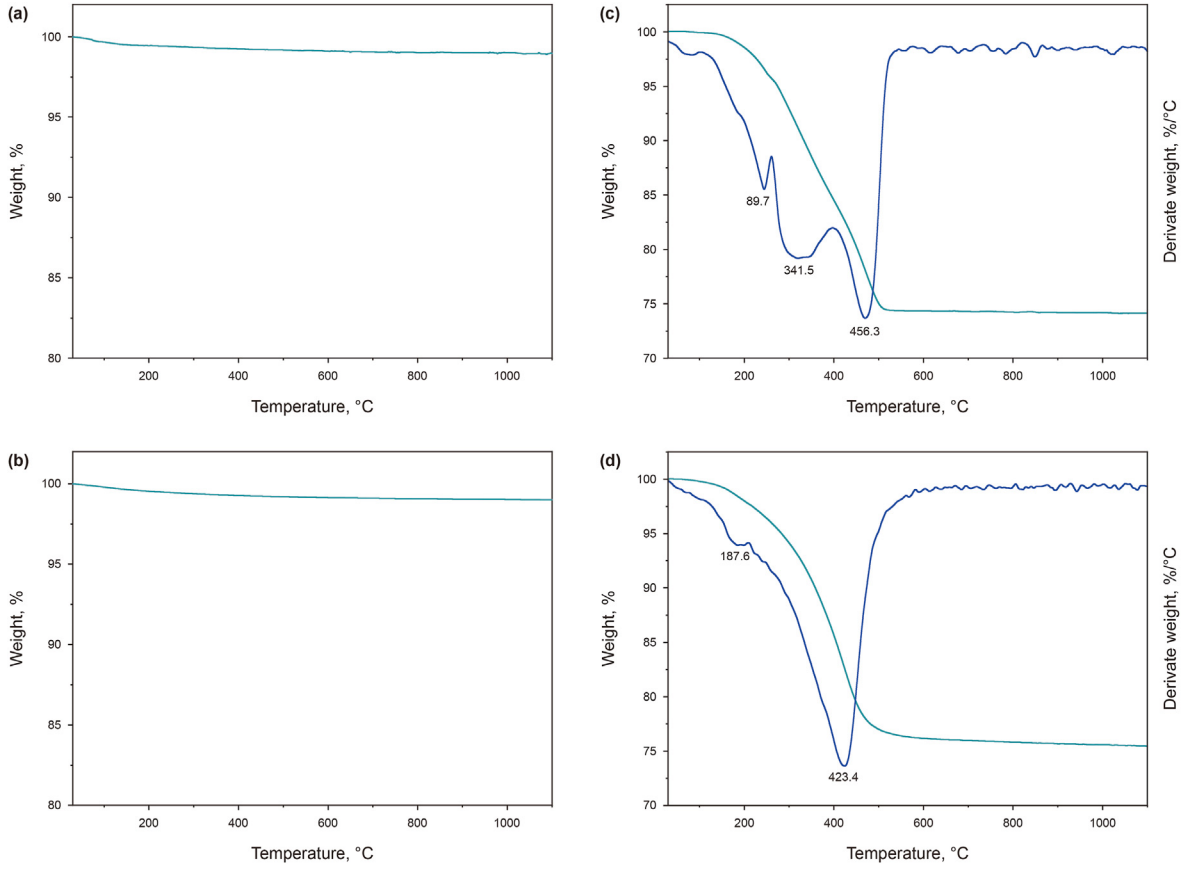

Fig. 3. TG profiles of fresh catalyst Cat-1 in (**a**) air atmosphere and (**b**) nitrogen atmosphere, TG profiles and differential curve of spent catalyst Cat-2 in (**c**) air atmosphere and (**d**) nitrogen atmosphere.

2.3. Structural characterization

Powder X-ray diffraction (XRD) patterns were recorded on Bruker D8 Advance diffractometer with a copper target at 40 kV, 40 mA, with a scanning angle of 5°–80° and scanning speed of 5°/min. The N_2-adsorption analysis was conducted on the Micromeritics ASAP 2460 physical adsorption instrument at −196 °C. The specific surface area (S_{BET}) was calculated according to the Brunauer-Emmett-Teller (BET) method. The pore size was calculated by Barrett-Joyner-Halenda (BJH) method. The contents of Pd and Ag were determined on Shimadzu inductively coupled plasma atomic emission spectrometer (ICP-AES9820). For better comparison, Cat-2 was regenerated by calcination at 500 °C to remove carbon deposit before the ICP test. The sample was digested with phosphoric acid-sulfuric acid with a molar ratio of 1:1. Microstructures of the samples were analyzed by FEI Talos F200X field emission high-resolution electron microscope with acceleration voltage 200 kV. High-angle annular dark field (HAADF) image and micro-area element distribution surface scan analysis (STEM-Mapping) were conducted on the same instrument. The sample was obtained by scraping the surface of catalyst particles and then dispersed ultrasonically in ethanol. Thermal analysis was carried out on Netzsch STA449 thermal analyzer from room temperature to 1100 °C with a heating rate of 10 °C/min. GC-MS analysis was conducted on ThermoFisher TRACE1300+ISQ7000 GC-MS. The sample was diluted with dichloromethane for sampling. The retention time was calibrated with the retention time of dichloromethane solvent of 3.6–3.7 min. XPS measurements were performed on a Thermo Fisher K-Aepra ESCA X-ray photoelectron spectrometer with Al Kα ray as the excitation source, and the binding energy was calibrated by C1s peak with the binding energy of 284.6 eV.

3. Results and discussion

3.1. Bulk structure analysis

XRD patterns of fresh catalyst Cat-1 and spent catalyst Cat-2 are shown in Fig. 2(b). Both catalysts exhibit similar patterns with characteristic diffraction peaks at 25.58°, 35.15°, 37.78°, 43.36°, 52.56°, 57.51°, 66.52°, 68.21° and 76.89°, and 16.22°, 19.59°, 31.21°, 31.61°, 31.70°, 32.78°, 36.68°, 38.88°, 40.05°, 44.80°, 47.59°, 59.90°, 63.93°, 67.42° and 67.57°, corresponding to α-Al_2O_3 (PDF 78-2462) and θ-Al_2O_3 (PDF 86-1410), indicating that both α-Al_2O_3 and θ-Al_2O_3 exist in the two catalysts and no observed phase change during the reaction. However, the presence of carbon deposit had some impact so that the XRD pattern intensity of Cat-2 slightly decreased compared to Cat-1. No obvious diffraction patterns are detected for Pd and Ag species, meaning a good dispersion of active metals even for spent catalyst Cat-2; this will be confirmed by TEM results with their average PdAg crystal size of 4 nm. Meanwhile, no apparent fragmentation or pulverization of catalyst particles is observed when the catalyst is unloaded in the plant (Fig. 2(a)), indicating that the fragmentation of catalyst particles and reactor blockage are not the reasons for the deactivation.

3.2. Carbon deposit analysis

Carbon deposit on the catalyst surface is an important cause of deactivation, so the carbon contents of Cat-1 and Cat-2 are analyzed with a carbon & sulfur analyzer. Cat-1 contains little carbon, while the carbon content of Cat-2 is as high as 13.76 wt%, indicating that

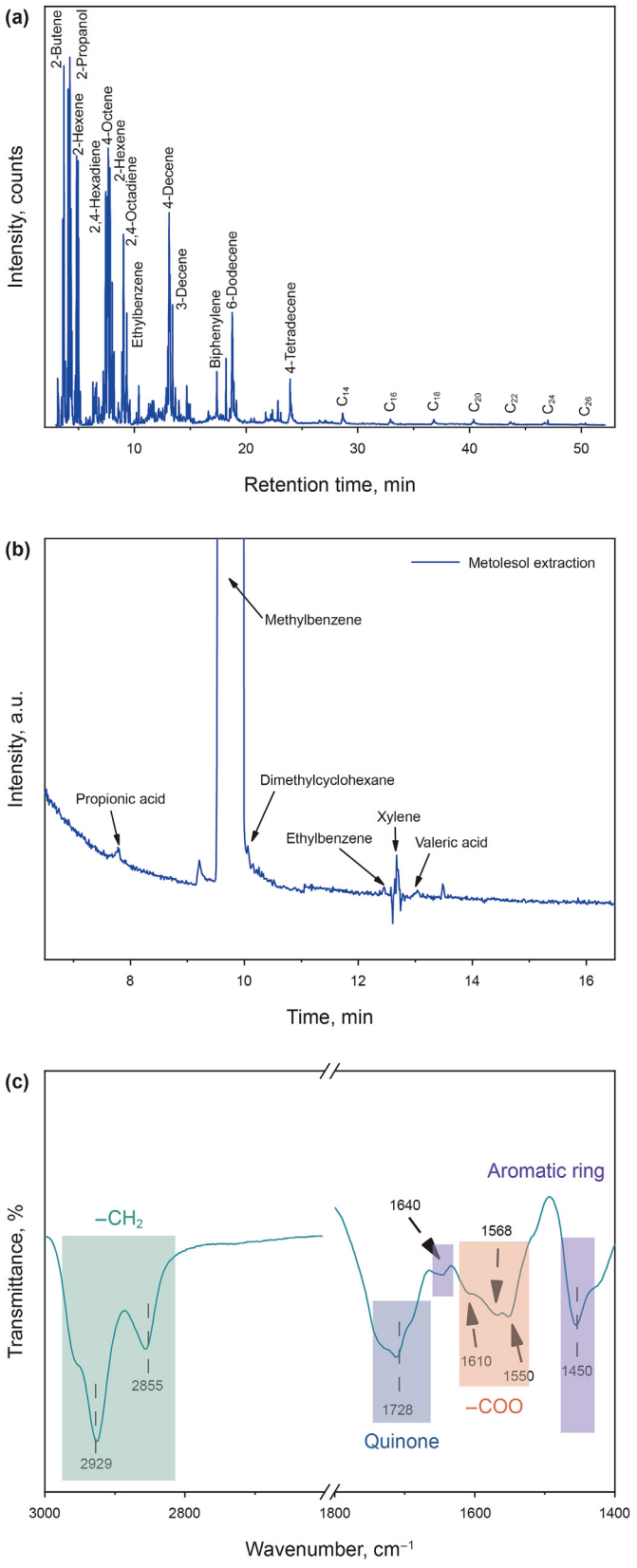

Fig. 4. (**a**) GC-MS of green oil, (**b**) GC-MS of toluene extracts, (**c**) FTIR spectrum of Cat-2 taking Cat-1 as the background.

the carbon deposit is severe during operation. During the reaction, acetylene will be polymerized to form liquid hydrocarbon mixtures called 'green oil' with various chain lengths and complicated compositions (Sarkany et al., 1984; Forzatti and Lietti, 1999; Huang and Chen, 2022; Zhang et al., 2016; Zhou et al., 2020) and the 'green oil' is the primary source of carbon deposit. Because of the large amount of green oil produced during the reaction, a green oil collecting tank is usually installed behind the reactor in an industrial plant to reduce the influence of green oil on the catalyst.

The deposited green oil, especially the long-chain components, can be further dehydrogenated and coked to form carbon deposits. It means that the carbonaceous material in the spent catalyst contains both green oil and carbon deposits. In order to obtain the information of green oil and carbon deposits, thermal analysis of Cat-1 and Cat-2 is conducted under air and nitrogen, respectively, and the results are shown in Fig. 3. Cat-1 has no noticeable weight loss in either air or nitrogen atmosphere (Fig. 3(a), (b)). In contrast to Cat-1, when Cat-2 is heated in an air atmosphere, a typical three-stage weight loss is observed (Abdulrasheed et al., 2019; Hansen et al., 2013; Forzatti and Lietti, 1999; Zhang et al., 2016) with peaks at 248.5, 342.5 and 456.3 °C (Fig. 3(c)). The first and second stages were mainly attributed to the vaporization of water and combustion of light green oil, while the third stage is mainly attributed to the combustion of heavy green oil and carbon deposits. No weight loss is observed from 456.3 to 1100 °C, indicating that water and carbonaceous materials in Cat-2 had been removed completely. In the N_2 atmosphere, Cat-2 also shows an apparent weight loss, peaking at ca. 423.4 °C with a small shoulder at 187.6 °C (Fig. 3(d)). Because combustion does not occur in the absence of oxygen, and the green oil and carbon deposits are removed through thermal decomposition and vaporization, the decomposition is not as complete as that in the air condition.

GC-MS analysis results of green oil (Fig. 4(a)) show that the green oil from the plant is mainly composed of alkanes and alkenes in the range of C_4–C_{26} (Huang and Chen, 2022). This means that the boiling point of each component of green oil is below 420 °C, indicating that the weight loss in the nitrogen atmosphere (Fig. 3(d)) is mainly due to the vaporization and decomposition of green oil. The results also indirectly indicate that the multi-stage weight loss of Cat-2 in the air is caused by the combustion of green oil and carbon deposits.

In order to further explore the information of deposits on Cat-2, toluene has been used for the Soxhlet extraction, and the toluene extract has been analyzed by GC-MS, as shown in Fig. 4(a), the presence of coking substances, including ethylbenzene, dimethylbenzene, pentanoic acid, propionic acid, dimethyl-cyclohexane, and cyclooctene. Meanwhile, the FTIR test of the spent catalyst has been taken with the fresh catalyst Cat-1 as the background, as shown in Fig. 4(c). Peaks at 1450 and 1640 cm^{-1} are associated with the stretching vibration of the phenyl ring (Wang et al., 2022). Peaks at 1550, 1568, and 1610 cm^{-1} are attributed to the stretching vibration of the –COO group, indicating the formation of carboxylic acids (Wang et al., 2020). Peaks at 2855 and 2928 cm^{-1} correspond to the stretching vibration of methyl groups (Wang et al., 2020). The peak at 1728 cm^{-1} corresponds to the stretching vibration of quinones (Wang et al., 2022). These results further confirm the formation of alkanes and aromatic compounds, which may be attributed to the polymerization of ethylene and aromatization processes.

3.3. Active metal analysis

Table 1 lists the contents of active metals Pd and Ag in Cat-1 and Cat-2. The results show that the metal content of Cat-1 and Cat-2 is approximately the same, indicating no noticeable loss of active metal components during the reaction. The loss of Ag is considered important for the permanent catalyst deactivation in previous reports (Zhang et al., 2017). However, no loss of active metal components has been observed from the ICP results in Table 1.

The surface elemental composition and active metal valence state of Cat-1 and Cat-2 are tested by XPS and shown in Fig. 5. From the full XPS spectra of the fresh and spent catalyst (Fig. 5(a)), the surface C content in spent catalyst Cat-2 is significantly higher than that of fresh catalyst Cat-1, which shows the same trends with the bulk carbon content by a carbon analyzer. The difference in carbon content tested by XPS and carbon analyzer is the surface and bulky carbon content, respectively. Nevertheless, the higher carbon content in Cat-2, as compared with Cat-1, indicates that a large number of carbonaceous materials were deposited on the surface of the spent catalyst, which is consistent with the results of the thermogravimetric analysis.

The Ag 3d and Pd 3d spectra (Fig. 5(b), (c)) show peaks attributed to metal Pd and Ag both appear in fresh catalyst Cat-1, while no peaks of Pd and Ag can be observed on the surface of Cat-2. The disappearance of Pd 3d and Ag 3d peaks may be due to the existence of a large number of deposited carbonaceous materials on the catalyst surface, covering the active metal sites (Sarkany et al., 1984). Meanwhile, the uneven distribution of metals caused by sintering cannot be ruled out. Thus, the surface metal species on Cat-2 are challenging to detect by XPS. It is worth noting that the binding energy of $Ag3d_{5/2}$ in Cat-1 is 367.6 eV, which is slightly smaller than 368.2 eV of elemental Ag (Fig. 5(b)); meanwhile, the binding energy of Pd $3d_{5/2}$ is 336.3 eV (Fig. 5(c)), which is slightly larger than 335.8 eV of elemental Pd, indicating that the active metals exist in the form of Pd–Ag alloy clusters or alloy nanoparticles (Ptáček and Bastl, 1990).

3.4. Textural properties

The textural properties of fresh and spent catalysts are compiled in Table 1. Compared with fresh catalyst Cat-1, the specific surface area (S_{BET}) and pore volume of spent catalyst Cat-2 decrease while the average pore size increases. This decrease in S_{BET} and pore volume and increase in average pore size can be explained by the existence of carbon deposits blocking the micropores of the catalyst. This is also an essential reason for catalyst deactivation (van Vegten et al., 2009). As shown above, no phase change appears between fresh and spent catalysts from the XRD results, and no

Table 1
Metal content and textural properties of Cat-1 and Cat-2.

Sample	Ag, wt%	Pd, wt%	S_{BET}, m^2/g	Pore volume, cm^3/g	Average pore diameter, nm
Cat-1	0.039	0.023	32	0.15	21.1
Cat-2	0.039	0.022	18	0.12	30.7

fragmentation of catalyst particles (Fig. 2(a)) and no active metal loss can be observed in Table 1; therefore, the decrease in S_{BET} and pore volume of spent catalyst can be attributed to carbon deposit on the surface, and the increase in the average pore size of Cat-2 indicates that the carbon deposits mainly block the small pores (Forzatti and Lietti, 1999).

3.5. Microstructural analysis

Scanning transmission electron microscopy (STEM) combined with high-angle annular dark field imaging (HAADF), can easily show the metal particles with a higher atomic number than the element Al in the support. Hence, they are widely used in the study of supported precious metal catalysts (Akita et al., 2010; He et al., 2022; Huang et al., 2022), especially for very fine nanoparticles which are difficult to be observed by transmission electron microscopy (TEM). Due to the high dispersion of active metals and the small size of metal nanoparticles of the acetylene hydrogenation catalyst, the active metal particles can hardly be observed by TEM (Zhang et al., 2017; Liu et al., 2017). Therefore, STEM-HAADF is used to analyze the dispersion of active metal particles, as shown in Fig. 6. For precise analysis, more than 100 nanoparticles in several STEM images have been included in the static analysis of average particle size. It was found that the nanoparticles of the active metals in Cat-1 are distributed very uniformly (Fig. 6(a)) with an average particle size of about 2.80 ± 0.07 nm (Fig. 6(b)), indicating that the active metals in Cat-1 have excellent dispersion. HRTEM shows lattice spacing of 0.23 nm of metal nanoparticles (Fig. 6(c)), which is between the spacing of Ag (111) of 0.2359 nm (PDF#040783) and the spacing of Pd (111) of 0.2246 nm (PDF#46-1043), indicating that Ag and Pd form Pd–Ag alloy nanoparticles (Huang et al., 1998; Zhang et al., 2000), which is consistent with the results of XPS. The uniformity of metal nanoparticles in Cat-2 becomes significantly worse (Fig. 6(d)). The average particle size is increased to about 4.30 ± 0.26 nm (Fig. 6(e)) with some particle sizes of 10 nm or even above 20 nm, and the metal sintering can be observed. Although the catalyst particle size increases after deactivation, the metal nanoparticles in Cat-2 still remain in the alloy state, as indicated by the HRTEM result (Fig. 6(f)). STEM area scanning element analysis (mapping) further confirms the Pd–Ag alloy state of active metal nanoparticles (Fig. 7). STEM-mapping shows that the distribution of Pd and Ag elements almost overlap, which proves the existence of Pd–Ag alloy (Huang et al., 1998; Zhang et al., 2000). Pd and Ag are adjacent elements in the periodic table, and they have similar atomic radii, and they both belong to the face-centered cubic crystal type and are easy to form alloys. At the same time, the binding energy of Pd–Ag (137 kJ/mol) is higher than that of Pd–Pd (100 kJ/mol), so Pd–Ag alloy has higher thermodynamic stability, which further ensures that Pd and Ag can remain in the alloy state (Xia et al., 2013; Gong et al., 2020).

Pd–Ag alloy is generally regarded as the active center for the selective hydrogenation of acetylene (Gong et al., 2020). The above results show that the metal particles in Cat-1 and Cat-2 are in the form of alloys, so the catalyst deactivation cannot be assigned to the metal separation of Pd and Ag. However, the metal particle size in Cat-2 is significantly larger than that of Cat-1, indicating that the sintering of metal particles is an essential reason for deactivation. The acetylene hydrogenation catalyst is used at a very low temperature, and the industrial operating temperature keeps below 80 °C. Under such mild reaction conditions, the possibility of sintering is very low. However, the catalyst must be regenerated frequently at hydrothermal conditions up to 500 °C (Pachulski et al.,

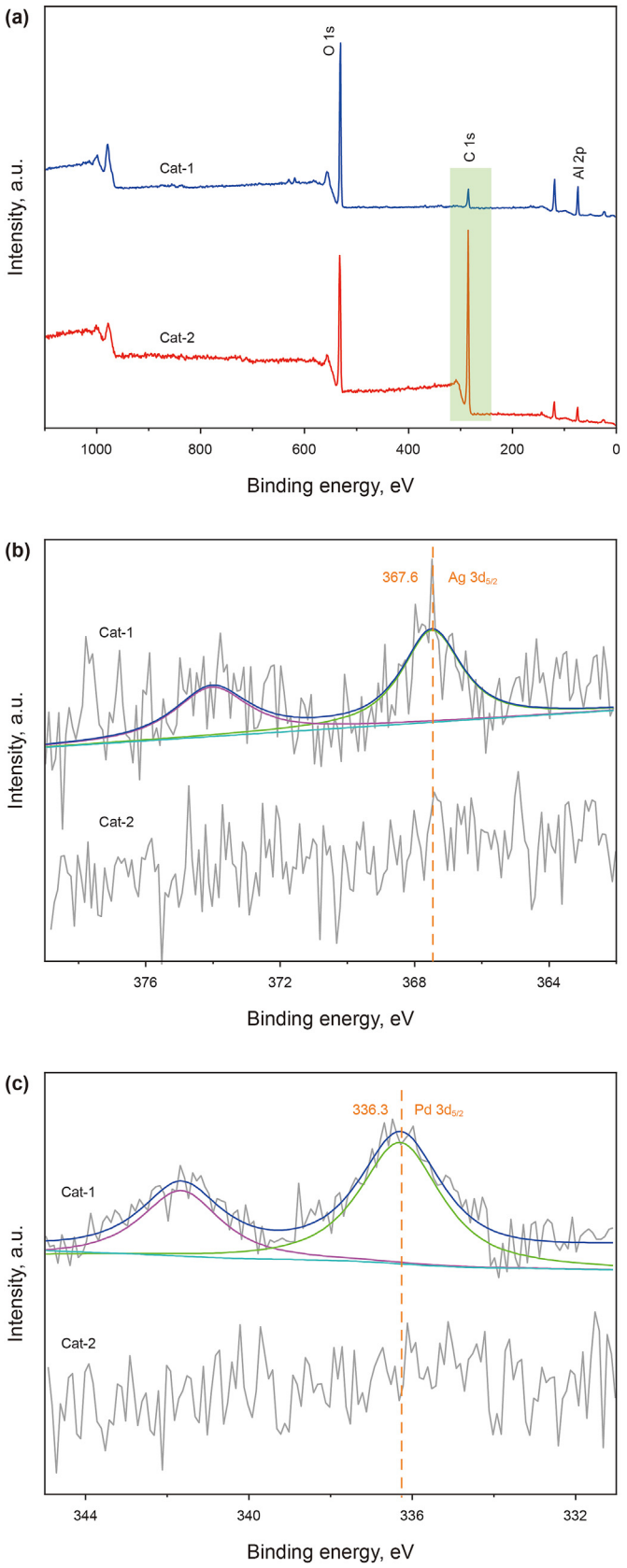

Fig. 5. (**a**) Full, (**b**) Ag 3d, (**c**) Pd 3d XPS spectra of fresh catalyst Cat-1 and spent catalyst Cat-2.

2011; Wang, 1995) to remove green oil and carbon deposits. Therefore, it is speculated that the sintering of metal nanoparticles is caused by the high temperature and the hydrothermal condition in the regeneration process. Usually, Pd particles are sintered at above 600 °C on the surface of alumina. Whereas, under the regeneration condition, due to the presence of water vapor and green oil, Pd particles are sintered at 500 °C (Liu et al., 2005). Meanwhile, the sintering temperature of nanoparticles will be significantly lower than bulk metals.

3.6. Evaluation results of model catalysts

The characterization results show that green oil, carbon deposit and sintering of metal particles might be the factors causing catalyst deactivation. In order for the role of each factor in deactivation, the catalytic performances of model catalysts with different influencing factors (Fig. 1) are studied under the same conditions. The evaluation results are shown in Fig. 8. The evaluation results of Cat-1 (Fig. 8(a)) show that the acetylene conversion increases rapidly with temperature and reaches almost 100% at 80 °C. However, the too-high temperature will lead to over-hydrogenation of acetylene, so the ethylene selectivity decreases at high temperatures. In industrial plants, low temperature is used at the early stage of the reaction, and increase the temperature later to compensate for the loss of activity. As shown in Fig. 8(a), it can be seen that Cat-2 has significantly lower acetylene conversion and ethylene selectivity as compared with Cat-1. Fig. 8(a) indicates that the Cat-2 has been seriously deactivated, and it is impossible to improve the performance by increasing the reaction temperature, which is a common strategy used in the industry (Chen et al., 2022b; Liu et al., 2005; Ma et al., 2020).

In order to elucidate the main reason for the deactivation, compared with fresh catalyst Cat-1, Cat-3 after fully dipping fresh catalyst Cat-1 in green oil, the acetylene conversion and ethylene selectivity of Cat-3 decreases dramatically (Fig. 8(b)), although the performance tends to improve with the increase of reaction temperature, there is still a significant difference in performance. However, the conversion of the catalyst Cat-4 recovers after further removing green oil from Cat-3, which is almost the same as before dipping green oil. The results suggest that green oil can reduce the catalytic activity; however, the deactivation is reversible, and the activity can recover after removing green oil (Fig. 8(b)). After the removal of green oil from Cat-2, the activity of Cat-5 increased obviously (Fig. 8(c)), indicating that the decrease in activity caused by green oil is reversible.

In order to distinguish the effects of carbon deposit and metal sintering, two methods are used to remove carbon deposits in Cat-2, i.e., calcination at 500 °C in the air (Cat-6) and calcination at 500 °C in air & steam with a prolonged time of 48 h (Cat-7). The performances of the corresponding model catalysts are shown in

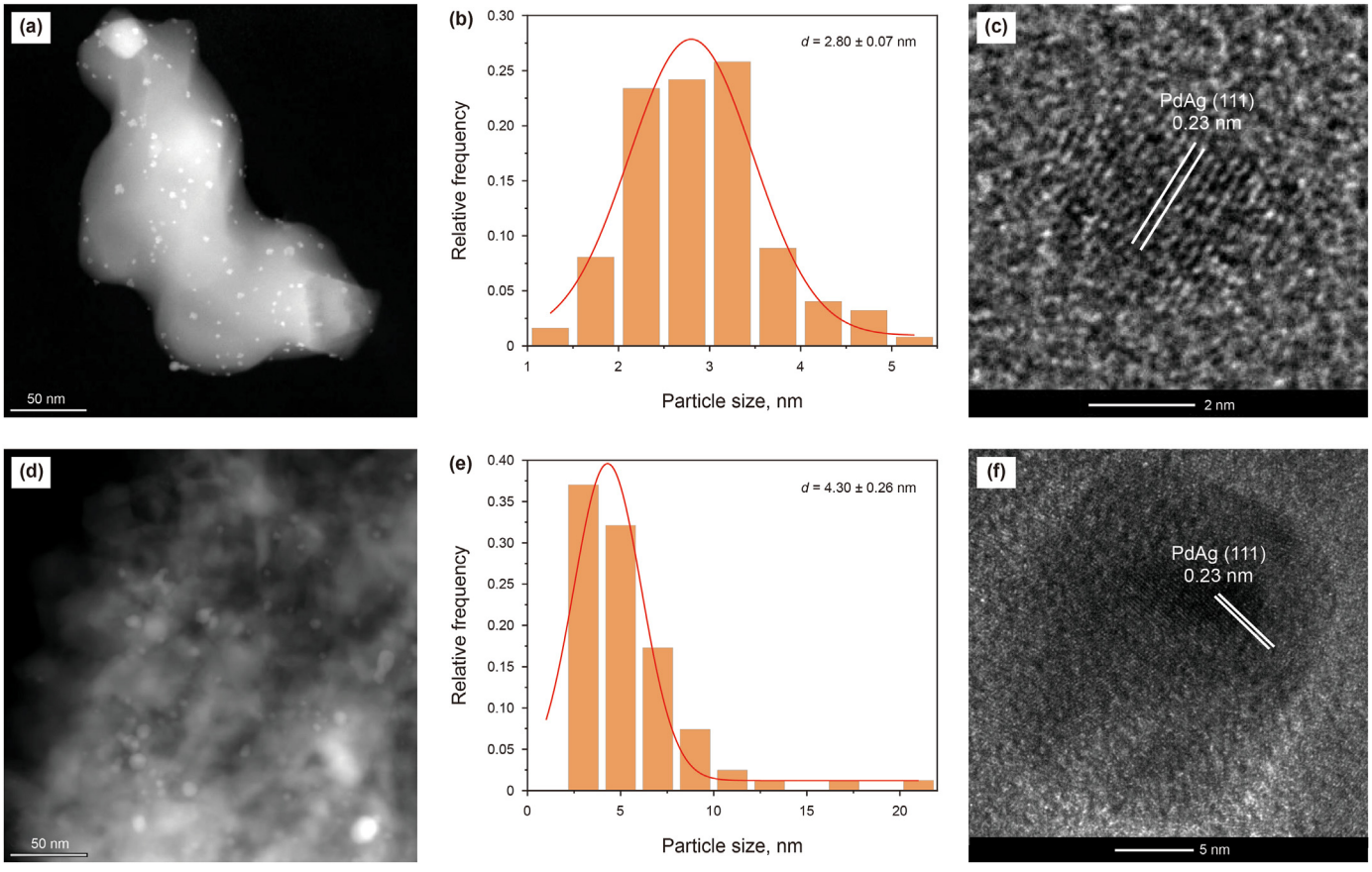

Fig. 6. (**a**) STEM-HAADF image of fresh catalyst Cat-1, (**b**) HRTEM image of resh catalyst Cat-1, (**c**) particle size distribution of fresh catalyst Cat-1, (**d**) STEM-HAADF image of fresh spent catalyst Cat-2, (**e**) HRTEM image of spent catalyst Cat-2, (**f**) particle size distribution of spent catalyst Cat-2.

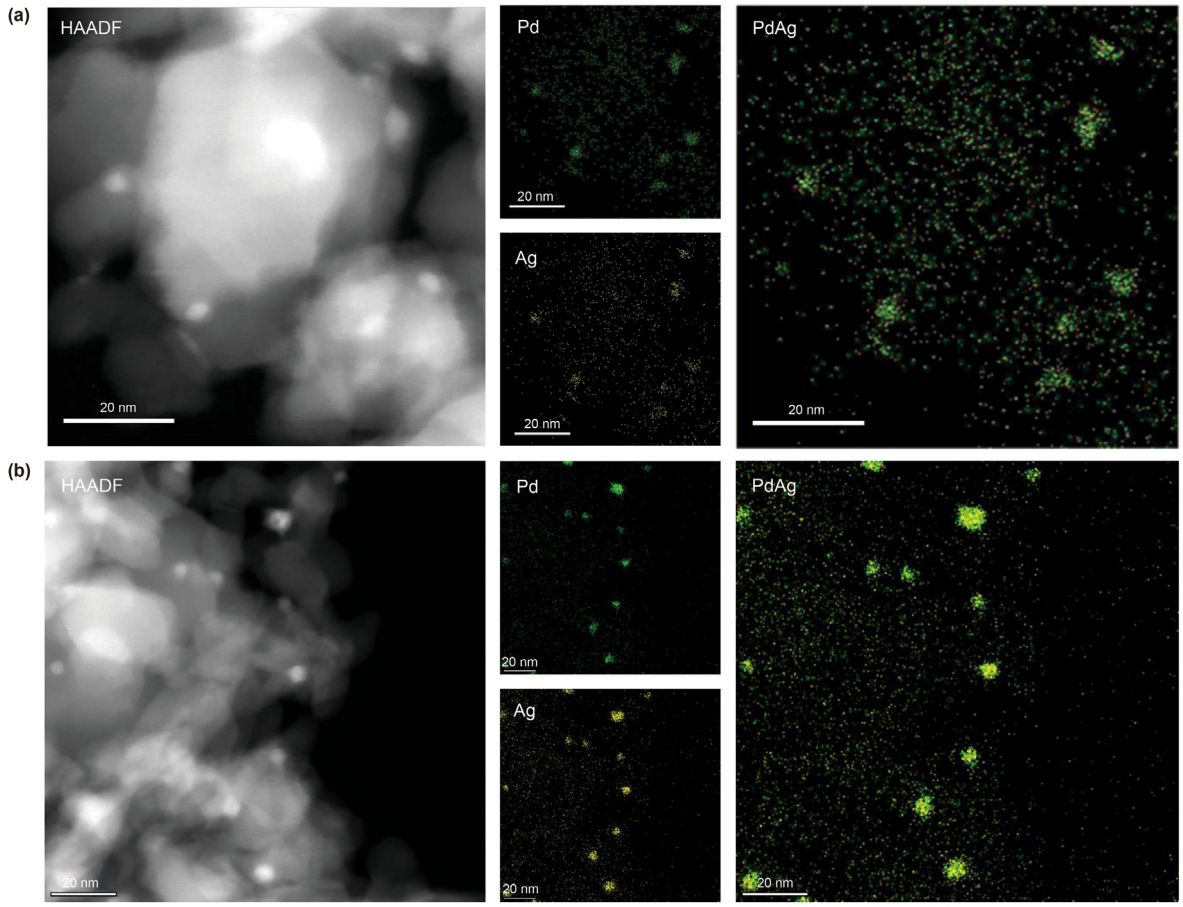

Fig. 7. HAADF images, distribution of Pd and Ag elements of (**a**) fresh catalyst Cat-1 and (**b**) spent catalyst Cat-2.

Fig. 8(c). Compared with Cat-2, the activities of Cat-6 were greatly improved, indicating that burning off carbon deposits is beneficial for the recovery of catalyst performance. However, if calcined Cat-2 under steam & air at a prolonged time, a noticeable decrease in the activity was observed, which might be attributed to the further sintering of metal particles during calcination under steam (Ahn et al., 2007; Liu et al., 2005) (Fig. 8(c)).

Based on the results of Fig. 8(a)–(c), it can be concluded that the green oil and carbon deposit, which covers the active sites of catalysts, triggers the decrease in reaction performance. However, the deactivation is reversible. Metal sintering is the main reason for the decrease in activity and ethylene selectivity and contributes much to the permanent deactivation of the catalyst. Although the operating conditions industrially are mild and do not cause the sintering of active metal particles, the catalyst needs to be frequently regenerated under hydrothermal conditions up to 500 °C in the long-term use of industrial plants (Pachulski et al., 2011; Liu et al., 2005). A recurrent regeneration using oxygen-containing regeneration gas may possibly be adopted to further remove green oil and carbon deposits (Liu et al., 2005; Wang, 1995). The harsh conditions of regeneration can lead to the sintering of metal particles, eventually, the permanent deactivation of the catalyst. Therefore, high-temperature hydrothermal regeneration and high-temperature recurrent regeneration in an oxygen-containing atmosphere are the primary causes of catalyst deactivation. To enhance the catalyst lifetime, it is necessary to optimize the catalyst regeneration process and develop more moderate regeneration conditions.

4. Conclusions

The studies of fresh commercial catalysts and spent catalysts unloaded from industrial plants show that the spent catalysts do not show fragmentation and no apparent phase change from XRD patterns of spent catalyst Cat-2, while the diffraction pattern intensity of Cat-2 slightly decreases, compared with Cat-1. No PdAg metals loss can be observed during the industrial operation. Green oil accumulation, carbon deposit, a reduction in the specific surface area of the support and the sintering of metal particles are the causes of catalyst deactivation; however, the deactivation caused by green oil and carbon deposit is reversible. However, the metal sintering and noticeable reduction in surface area and pore volume of the catalysts are important factors leading to a decrease in activity and selectivity, finally resulting in the permanent deactivation of the catalyst. Since sintering originates from the high-temperature hydrothermal regeneration process, optimizing the regeneration process and developing mild regeneration conditions are challenging to improve the catalyst lifetime further.

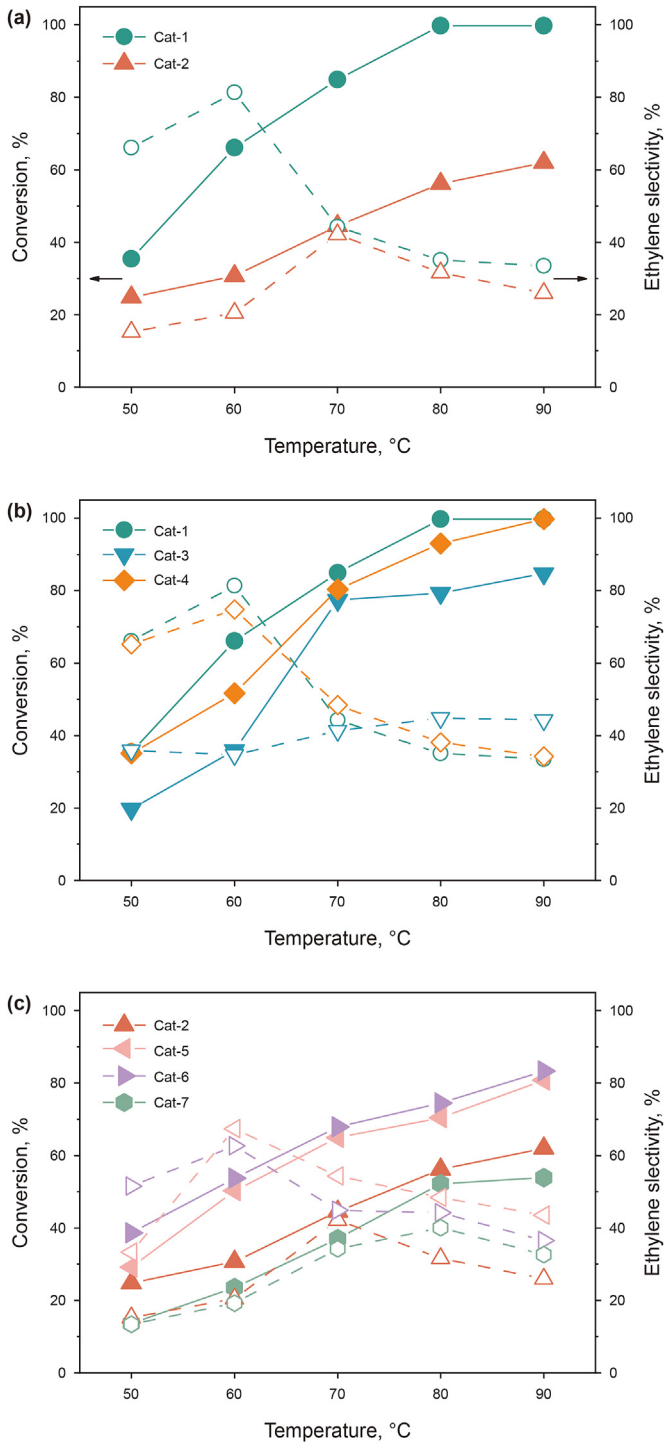

Fig. 8. Conversion and selectivity of (**a**) Cat-1 and Cat-2, (**b**) Cat-1 and Cat-3 (after introducing green oil on Cat-1) & Cat-4 (further removal of green oil from Cat-3), (**c**) Cat-2, Cat-5 (after toluene extraction of Cat-2), Cat-6 (calcination of Cat-2 at 500 °C for 4 h), and Cat-7 (Calcination of Cat-2 under steam & air at 500 °C for 48 h).

Declaration of competing interest

The authors declare that they have no known competing financial interests or personal relationships that could have appeared to influence the work reported in this paper.

Acknowledgments

The authors would like to thank the financial support from the Sinopec Catalyst Co. Ltd., China.

References

Abdulrasheed, A., Jalil, A.A., Gambo, Y., et al., 2019. A review on catalyst development for dry reforming of methane to syngas: recent advances. Renew. Sustain. Energy Rev. 108, 175–193. https://doi.org/10.1016/j.rser.2019.03.054.

Ahn, I., Lee, J., Kum, S., et al., 2007. Formation of C4 species in the deactivation of a Pd/SiO_2 catalyst during the selective hydrogenation of acetylene. Catal. Today 123, 151–157. https://doi.org/10.1016/j.cattod.2007.02.011.

Akita, T., Tanaka, K., Kohyama, M., et al., 2010. HAADF-STEM observation of Au nanoparticles on TiO_2. Surf. Interface Anal. 40 (13), 1760–1763. https://doi.org/10.1002/sia.2999.

Borodziński, A., Bond, G.C., 2006. Selective hydrogenation of ethyne in ethene-rich streams on palladium catalysts. Part 1. Effect of Changes to the Catalyst during Reaction. Catal. Rev. Sci. Eng. 48 (2), 91–144. https://doi.org/10.1080/01614940500364909.

Che, C., Gou, G., Wen, H., et al., 2020. Study on the reaction mechanism of acetylene selective hydrogenation catalysts $Pd-Ag/Al_2O_3$. Inorg. Nano-Metal Chem. 51 (1), 70–77. https://doi.org/10.1080/24701556.2020.1762217.

Chen, Z.Q., Wu, D.F., Wen, H., et al., 2022a. Advances in catalysts for selective hydrogenation of acetylene. Chem. Ind. Eng. Prog. 1–18. https://doi.org/10.16085/j.issn.1000-6613.2021-2568.

Chen, Z.Q., Che, C.X., Wu, D.F., et al., 2022b. Effect of Al_2O_3 support modification on acetylene hydrogenation catalyst. Petrochem. Technol. 51 (11), 1269–1276. https://doi.org/10.3969/j.issn.1000-8144.2022.11.002 (in Chinese).

Dehghani, O., Rahimpour, M., Shariati, A., 2019. An experimental approach on industrial Pd-Ag supported α-Al_2O_3 catalyst used in acetylene hydrogenation process: mechanism, kinetic and catalyst decay. Processes 7 (3), 136. https://doi.org/10.3390/pr7030136.

Forzatti, P., Lietti, L., 1999. Catalyst deactivation. Catal. Today 52, 17. https://doi.org/10.1016/S0920-5861(99)00074-7.

Glyzdova, D.V., Afonasenko, T.N., Khramov, E.V., et al., 2020a. Liquid-phase acetylene hydrogenation over Ag-modified Pd/Sibunit catalysts: effect of Pd to Ag molar ratio. Appl. Catal. Gen. 600. https://doi.org/10.1016/j.apcata.2020.117627.

Glyzdova, D.V., Afonasenko, T.N., Khramov, E.V., et al., 2020b. Zinc addition influence on the properties of Pd/Sibunit catalyst in selective acetylene hydrogenation. Top. Catal. 63 (1–2), 139–151. https://doi.org/10.1007/s11244-019-01215-9.

Glyzdova, D.V., Afonasenko, T.N., Khramov, E.V., et al., 2021. Effect of pretreatment with hydrogen on the structure and properties of carbon-supported Pd-Ag-nanoalloys for ethylene production by acetylene hydrogenation. Mol. Catal. 511. https://doi.org/10.1016/j.mcat.2021.111717.

Gonçalves, L., Wang, J., Vinati, S., et al., 2020. Combined experimental and theoretical study of acetylene semi-hydrogenation over Pd/Al_2O_3. Int. J. Hydrogen Energy 45 (2), 1283–1296. https://doi.org/10.1016/j.ijhydene.2019.04.086.

Gong, X., Song, L.J., Qing, Y.C., 2020. C_4 olefins generation rules on Pd-Ag catalyst for acetylene selective hydrogenation. J. Liaoning Shihua Univ. 40 (5). https://doi.org/10.3969/j.issn.1672-6952.2020.03.007 (in Chinese).

Guo, Y., Qi, H., Su, Y., et al., 2021. High performance of single-atom catalyst Pd_1/MgO for semi-hydrogenation of acetylene to ethylene in excess ethylene. ChemNanoMat 7 (5), 526–529. https://doi.org/10.1002/cnma.202100037.

Hansen, T.W., Delariva, A.T., Challa, S.R., et al., 2013. Sintering of catalytic nanoparticles: particle migration or Ostwald ripening? Accounts Chem. Res. 46 (8), 1720–1730. https://doi.org/10.1021/ar3002427.

He, C., Yuan, M., Jiang, B., et al., 2022. Improving the isotropy and formability of extruded Mg-2Gd-1Zn (wt.%) alloy sheet by introducing an ellipse texture. Mater. Sci. Eng., A 836, 142699. https://doi.org/10.1016/j.msea.2022.142699.

Hou, C.L., Kang, L.H., Li, H.L., 2023. Density functional theory study on $Ni_1/g-C_3N_4$ catalytic hydrogenation of acetylene. J. Shihezi Univ. 1–8. https://doi.org/10.13880/j.cnki.65-1174/n.2023.22.008 (in Chinese).

Hu, M., Wu, Z., Yao, Z., et al., 2021. N8 stabilized single-atom Pd for highly selective hydrogenation of acetylene. J. Catal. 395, 46–53. https://doi.org/10.1016/j.jcat.2020.12.009.

Huang, Y., Chen, Z.X., 2022. Alloying effect on the C–C coupling reactions in acetylene hydrogenation by palladium-coinage metal alloys, a DFT study and microkinetic modeling. Appl. Surf. Sci. 575. https://doi.org/10.1016/j.apsusc.2021.151513.

Huang, D., Chang, K., Pong, W., et al., 1998. Effect of Ag-promotion on Pd catalysts by XANES. Catal. Lett. 53 (3), 155–159.

Huang, X., Huang, L., Yan, H., et al., 2018. Toward understanding of the support effect on Pd1 single-atom-catalyzed hydrogenation reactions. J. Phys. Chem. C 123 (13), 7922–7930. https://doi.org/10.1021/acs.jpcc.8b07181.

Huang, X., Wang, Y., Wang, Q., et al., 2022. Highly efficient removal of tetracycline hydrochloride by CuNi-C MOF: activation of oxygen via radical and non-radical pathways. Separ. Purif. Technol. 290, 120860. https://doi.org/10.1016/j.seppur.2022.120860.

Kim, W.J., Shin, E.W., Kang, J.H., et al., 2003. Performance of Si-modified Pd catalyst in acetylene hydrogenation: catalyst deactivation behavior. Appl. Catal. Gen. 251 (2), 305–313. https://doi.org/10.1016/s0926-860x(03)00367-3.

Li, Q., Wang, Y., Skoptsov, G., et al., 2019a. Selective hydrogenation of acetylene to ethylene over bimetallic catalysts. Ind. Eng. Chem. Res. 58 (45), 20620–20629. https://doi.org/10.1021/acs.iecr.9b04604.
Li, X., Huang, Y., Liu, B., et al., 2019b. Catalyst: single-atom catalysis: directing the way toward the nature of catalysis. Chem 5 (11), 2733–2735. https://doi.org/10.1016/j.chempr.2019.10.004.
Liu, R.J., Crozier, P.A., Smith, C.M., et al., 2005. Metal sintering mechanisms and regeneration of palladium/alumina hydrogenation catalysts. Appl. Catal. Gen. 282 (1–2), 111–121. https://doi.org/10.1016/j.apcata.2004.12.015.
Liu, Z., Epicier, T., Lefkir, Y., et al., 2017. HAADF-STEM characterization and simulation of nanoparticle distributions in an inhomogeneous matrix. J. Microsc. 266 (1), 60–68. https://doi.org/10.1111/jmi.12519.
Liu, X., Huang, L., Zhu, Q., et al., 2022. Progress in palladium catalysts for acetylene semi-hydrogenation. Mater. Rev. 36 (20), 253–261. https://doi.org/10.11896/cldb.20090171 (in Chinese).
López, N., Vargas-Fuentes, C., 2012. Promoters in the hydrogenation of alkynes in mixtures: insights from density functional theory. Chem. Commun. 48 (10), 1379–1391. https://doi.org/10.1039/C1CC14922A.
Ma, S.L., Qin, H.L., Wang, X.G., et al., 2020. Operation analysis of C2 hydrogenation catalyst in ethylene plant. Ethylene Indust. 32 (4), 5.
Melnikov, D., Stytsenko, V., Saveleva, E., et al., 2020. Selective hydrogenation of acetylene over Pd-Mn/Al_2O_3 Catalysts. Catalysts 10 (6). https://doi.org/10.3390/catal10060624.
Méndez, F.J., Alves, J.A., Rojas-Challa, Y., et al., 2021. An egg-shell bifunctional CeO_2-modified NiPd/Al_2O_3 catalyst for petrochemical processes involving selective hydrogenation and hydroisomerization. J. Rare Earths 39 (11), 1382–1388. https://doi.org/10.1016/j.jre.2020.09.017.
Pachulski, A., Schödel, R., Claus, P., 2011. Performance and regeneration studies of Pd-Ag/Al_2O_3 catalysts for the selective hydrogenation of acetylene. Appl. Catal. Gen. 400 (1–2), 14–24. https://doi.org/10.1016/j.apcata.2011.03.019.
Ptáček, P., Bastl, Z., 1990. XPS characterization of supported bimetallic palladium-silver clusters. Appl. Surf. Sci. 45 (4), 319–323, 1016/0169-4332(90)90041-W.
Qi, Y., Wang, B., Fan, M., et al., 2021. C_2H_2 semi-hydrogenation on the metal M (M=Cu, Ag, Au) alloyed single-atom Pd catalysts: effects of Pd coordination number and environment on the catalytic performance. Chem. Eng. Sci. 243. https://doi.org/10.1016/j.ces.2021.116786.
Rassolov, A.V., Bragina, G.O., Baeva, G.N., et al., 2020. Formation of isolated single-atom Pd1 sites on the surface of Pd–Ag/Al_2O_3 bimetallic catalysts. Kinet. Catal. 61 (5), 758–767. https://doi.org/10.1134/s0023158420050080.
Ravindran, K., Madhu, G., Renjith, V.R., et al., 2023. Performance of the ρ-Al_2O_3 based Ag promoted Pd/Al_2O_3 catalyst during acetylene hydrogenation with an ideal feed. J. Indian Chem. Soc. 100 (2), 100884. https://doi.org/10.1016/j.jics.2023.100884.
Ren, J., Wu, Y.A., Shi, J.G., et al., 2021. Automatic Impregnation System for Catalyst Support. CN215353475U [P/OL] (in Chinese).
Ru, W., 2021. Regulating the local fine structure of Pd single-atom catalysts for selective hydrogenation of acetylene. PhD Dissertation. Beijing University of Chemical Technology (in Chinese).
Sarkany, A., Szilagyi, T., Sandor, O., et al., 1984. Green oil poisoning of a Pd/A1$_2O_3$ acetylene hydrogenation catalyst. Appl. Catal. 373–379. https://doi.org/10.1016/j.rser.2019.03.054.
Shi, J.G., Ren, J., Su, H.X., et al., 2022a. Alumina Carrier, Preparation Method and Application Thereof and Hydrogenation Catalyst Thereof. CN115178252A [P/OL] (in Chinese).
Shi, J.G., Ren, J., Su, H.X., et al., 2022b. Alumina Carrier, Preparation Method and Application Thereof and C_2 Hydrogenation Catalyst. CN115178251A [P/OL] (in Chinese).
Shi, J.G., Ren, J., Zheng, J.B., et al., 2022c. Hydrogenation Catalyst and Catalyst Support, Preparation Method and Application Thereof. CN114797854A [P/OL] (in Chinese).
Shi, J.G., Su, H.X., Ren, J., et al., 2022d. Preparation Method and Application of C2 Catalyst and C2 Catalyst Thereof. CN115178262A [P/OL] (in Chinese).
Shi, J.G., Zheng, J.B., Ren, J., et al., 2022e. Catalyst for Conversion of Alkynes to Alkenes, Preparation Method and Application Thereof. CN115178263A [P/OL] (in Chinese).
Tan, D.P., Wang, H.J., Che, C.X., et al., 2009. Causes for coke formation on C_2 hydrogenation catalysts and its countermeasures. Ind. Catal. 17 (3), 38–41 (in Chinese).
Tan, D.P., Gong, H.G., Zhang, X.Q., et al., 2023. Acetylene Removal Method for Light Hydrocarbon Cracking C2-Fraction by Selective Hydrogenation Process. CN112939717B [P/OL] (in Chinese).
Van Vegten, N., Maciejewski, M., Krumeich, F., et al., 2009. Structural properties, redox behaviour and methane combustion activity of differently supported flame-made Pd catalysts. Appl. Catal. B Environ. 93 (1–2), 38–49. https://doi.org/10.1016/j.apcatb.2009.09.010.
Wang, J., 1995. Optimization of regeneration mode of carbon dehydrogenation catalyst. LanHua Technol. 13 (4) (in Chinese).
Wang, A., Li, J., Zhang, T., 2018. Heterogeneous single-atom catalysis. Nat. Rev. Chem. 2 (6), 65–81. https://doi.org/10.1038/s41570-018-0010-1.
Wang, X.T., Sun, Y.L., Li, M.Y., et al., 2022. Catalysis Science and Technology. The Royal Society of Chemistry 12 (9), 2872–2886. https://doi.org/10.1039/d2cy00032f.
Wang, Y., Wang, B., Ling, L., et al., 2020. Probe into the effects of surface composition and ensemble effect of active sites on the catalytic performance of C_2H_2 semi-hydrogenation over the Pd-Ag bimetallic catalysts. Chem. Eng. Sci. 218. https://doi.org/10.1016/j.ces.2020.115549.
Wu, Y.A., Ren, J., Zhu, P., et al., 2019. Catalyst Carrier Forming System with Horizontal Type. CN208727517U [P/OL] (in Chinese).
Xia, X., Wang, Y., Ruditskiy, A., et al., 2013. 25th anniversary article: galvanic replacement: a simple and versatile route to hollow nanostructures with tunable and well-controlled properties. Adv. Mater 25 (44), 6313–6333. https://doi.org/10.1002/adma.201302820.
Yang, B., Burch, R., Hardacre, C., et al., 2013. Influence of surface structures, subsurface carbon and hydrogen, and surface alloying on the activity and selectivity of acetylene hydrogenation on Pd surfaces: a density functional theory study. J. Catal. 305, 264–276. https://doi.org/10.1016/j.jcat.2013.05.027.
Yang, L., Shi, J.G., Su, H.X., et al., 2021. Research and application progress of hydrorefining catalysts for cracking C2 fraction from ethylene in China. China Synth. Resin Plast. 38 (3), 64–70. https://doi.org/10.19825/j.issn.1002-1396.2021.03.13 (in Chinese).
Zhang, Q., Li, J., Liu, X., et al., 2000. Synergetic effect of Pd and Ag dispersed on Al_2O_3 in the selective hydrogenation of acetylene. Appl. Catal. Gen. 197 (2), 221–228. https://doi.org/10.1016/S0926-860X(99)00463-9.
Zhang, J.S., Zhu, Z.J., Chen, Y.A., et al., 2016. Composition of the green oil in hydrogenation of acetylene over a commercial Pd-Ag/Al_2O_3 catalyst. Chem. Eng. Technol. 39 (5), 865–873. https://doi.org/10.1002/ceat.201600020.
Zhang, J., Huang, B., Sui, Z., et al., 2017. The characterization of the deactivated C2 hydrogenation Pd-Ag/Al_2O_3 catalyst. Petrochem. Technol. 46 (7), 839–844. https://doi.org/10.3969/j.issn.1000-8144.2017.07.001.
Zhang, J., Huang, B., Sui, Z., et al., 2018. Microkinetic analysis of acetylene hydrogenation over Pd-Ag/Al_2O_3 catalyst with different Pd/Ag ratios. CIESC J. 69 (2), 674–681. https://doi.org/10.11949/j.issn.0438-1157.20171007 (in Chinese).
Zhang, X.J., Yin, G.H., Zheng, J.B., et al., 2022. Alumina Carrier, and Selective Hydrogenation Catalyst Thereof for C2 and C3 Fractions. CN111375451B [P/OL] (in Chinese).
Zhou, S., Kang, L., Xu, Z., et al., 2020a. Catalytic performance and deactivation of Ni/MCM-41 catalyst in the hydrogenation of pure acetylene to ethylene. RSC Adv. 10 (4), 1937–1945. https://doi.org/10.1039/c9ra09878j.
Zhou, S., Kang, L., Zhou, X., et al., 2020b. Pure acetylene semihydrogenation over Ni-Cu bimetallic catalysts: effect of the Cu/Ni ratio on catalytic performance. Nanomaterials 10 (3), 509. https://doi.org/10.3390/nano10030509.
Zhou, J., Xu, L., Huang, W., et al., 2022. Modification of the structure and catalytic performance of selective acetylene hydrogenation catalyst. Acta Pet. Sin. 38 (2), 467. https://doi.org/10.3969/j.issn.1001-8719.2022.02.025.